Journal of Magnetic Resonance 310 (2020) 106625

Contents lists available at ScienceDirect

Journal of Magnetic Resonance

journal homepage: www.elsevier.com/locate/jmr

Design and implementation of a low-cost, tabletop MRI scanner for education and research prototyping

Clarissa Zimmerman Cooley [a,b,*], Jason P. Stockmann [a,b], Thomas Witzel [a,b], Cris LaPierre [a], Azma Mareyam [a], Feng Jia [c], Maxim Zaitsev [c], Yang Wenhui [d], Wang Zheng [d], Pascal Stang [e,f], Greig Scott [f], Elfar Adalsteinsson [g,h], Jacob K. White [g], Lawrence L. Wald [a,b,h]

[a] A. A. Martinos Center for Biomedical Imaging, Department of Radiology, Massachusetts General Hospital, Charlestown, MA, USA
[b] Harvard Medical School, Boston, MA, USA
[c] Dept. of Radiology, Medical Physics, Medical Center University of Freiburg, Faculty of Medicine, University of Freiburg, Freiburg, Germany
[d] Institute of Electrical Engineering, Chinese Academy of Sciences, Beijing, China
[e] Procyon Engineering, San Jose, CA, USA
[f] Department of Electrical Engineering, Stanford University, Stanford, CA, USA
[g] Department of Electrical Engineering and Computer Science, Massachusetts Institute of Technology, Cambridge, MA, USA
[h] Harvard-MIT Division of Health Sciences Technology, Cambridge, MA, USA

ARTICLE INFO

Article history:
Received 16 July 2019
Revised 19 October 2019
Accepted 20 October 2019
Available online 22 October 2019

Keywords:
MRI
Portable
Low-cost
Educational

ABSTRACT

While access to a laboratory MRI system is ideal for teaching MR physics as well as many aspects of signal processing, providing multiple MRI scanners can be prohibitively expensive for educational settings. To address this need, we developed a small, low-cost, open-interface tabletop MRI scanner for academic use. We constructed and tested 20 of these scanners for parallel use by teams of 2–3 students in a teaching laboratory. With simplification and down-scaling to a 1 cm FOV, fully-functional scanners were achieved within a budget of $10,000 USD each. The design was successful for teaching MR principles and basic signal processing skills and serves as an accessible testbed for more advanced MR research projects. Customizable GUIs, pulse sequences, and reconstruction code accessible to the students facilitated tailoring the scanner to the needs of laboratory exercise. The scanners have been used by >800 students in 6 different courses and all designs, schematics, sequences, GUIs, and reconstruction code is open-source.

1. Introduction

A multi-institutional collaborative effort was made to design and build a set of 20 small low-cost educational MRI scanners for an undergraduate teaching lab at MIT. The design constraints included: (1) a budget of $10 k per scanner, (2) an imaging volume of 1 cm^3, (3) a portable design (all components fit on a small cart for transport into a teaching laboratory), (4) a robust, low maintenance design with passive air cooling and standard electrical supply, (5) an open, transparent design that could be made fully available to the students and community. The motivation for the scaled construction of 20 scanners was to allow a full laboratory section of about 60 students to perform experiments simultaneously in small groups. Comparable commercial benchtop MRI scanner are available from Pure Devices (Rimpar, Germany) [1], Magritek (Wellington, New Zealand), and Niumag (Shanghai, China). However, these scanners were not available near our price point and they do not offer the desired flexibility and transparency for our application. We note that the budget of $10 k per scanner was for raw materials, "parts-cost" only.

In addition, to the commercial tabletop scanners, there are relevant published tabletop and/or low-cost NMR/MR research systems. There are several compact, small FOV MRI systems from the University of Tsukuba, including a 1T "MR microscope", which used a 80 kg NdFeB dipole magnet to produce 3D images with 50μm isotropic resolution [2]. A compact mouse MRI was also published using a 1T yokeless permanent magnet with a 35 mm × 50 mm imaging volume [3]. A similar 1T yokeless magnet was used in a compact MRI system (installed in 0.6 m × 1.2 m space) for measuring trabecular bone microstructure in the finger [4]. A $13,500 desktop MRI system was published by Wright et al [5] in 2002. The system used a 0.21T C-shape permanent magnet with an imaging FOV of 2.5 cm, and was capable of

* Corresponding author.
E-mail address: clarissa@nmr.mgh.harvard.edu (C.Z. Cooley).

https://doi.org/10.1016/j.jmr.2019.106625
1090-7807/

producing 3D images of a fixed newborn mouse. Another 0.5T tabletop system was presented by Hasselwander et al, with a focus on a low-cost console development using software defined radios (SDR) [6]. There are also several examples of low-cost benchtop and mobile NMR systems for relaxometry and spectroscopy [7]. Including systems using miniature Halbach magnets [8,9], "MR-on-a-chip" systems [10] and single sided/ ex-situ systems [11–14].

These previously described MRI systems, while compact, do not meet our required classroom specification due to size or cost or lack full details for large-scale replication. Our presented scanner design (and most individual components) is offered as "open-source", with an open parts list, board files, library of pulse sequences, reconstruction code and user interface code to allow improvement and customization by the educational community. These resources are included as supplementary material, and will be maintained and updated on an on-line repository [15].

2. Educational uses of the scanner

While many courses teach the principles of Magnetic Resonance Imaging, using a clinical scanner as a hands-on teaching tool is generally not feasible. If available, it is an expensive redirection of clinical resources, at best only offering a single shared scanner to the class. Additionally, the hardware and software are relatively inflexible and hard to examine, hindering a deep understanding of the MRI system and its functionality. To address these issues, we set out to create a transparent teaching device with simplified hardware and software to reduce cost and increase accessibility. At the time of publication, the fleet of 20 educational scanners has been used for 6 years in 6 different courses at MIT by over 800 students. These dedicated tabletop scanners were found to be useful for teaching MR physics, hardware design, and data acquisition and image reconstruction techniques.

In addition to teaching MR-specific principles, the scanners are a useful vehicle for teaching more basic engineering topics. The scanners were originally developed for an undergraduate course titled "Introduction to Electrical Engineering and Computer Science (EECS) via Medical Technology". As the title implies, the students were new to both EECS and MRI topics. In this case, the scanners were used for the hands-on acquisition of a biomedical signal, which results in a more tangible and relevant way for teaching general signal processing concepts such as sampling theory, filtering, apodization, and the properties of the Fourier transform. Further, the scanners served as a concrete model of a biomedical instrument transparently broken up into components for exploration. The course design included MATLAB GUIs (graphical user interfaces) for each lab exercise, which enabled straightforward educational experiments and direct processing of data in the MATLAB environment (Mathworks, Natick, MA, USA). The availability of 20 scanners allowed for small groups (2–3 students) to have their own MRI scanner in the lab, granting each student ample hands-on time with the system.

In addition to the basic engineering course described above, the scanners have been used in 5 other MIT courses. "Magnetic Resonance Analytic, Biochemical, and Imaging Techniques" (HST.584) is a graduate course that touches upon all topics of MRI including physics, hardware, pulse sequences, image contrast, and image reconstruction. Laboratory exercises with the scanners enhance this course by solidifying the theoretical concepts and demonstrating hardware. Similarly, the scanners are used in "Data Acquisition and Image Reconstruction in MRI" (6.556), a more focused graduate EECS course. This course also includes a final project component, in which students have developed new pulse sequences for the scanners, some of which are now incorporated into the standard teaching GUIs. "Neurotechnology in Action" (9.123) introduces students to a range of cutting-edge neurotechnology methods. A module dedicated to fMRI is enriched by laboratory exercises with the scanners, giving students a hands-on introduction to MRI principles. The scanners have also been used in "Instrumentation and Measurement of Biological Systems" (20.309), a bioengineering undergraduate laboratory course that exposes students to bioinstrumentation through guided and independent laboratory projects. Finally, the scanners are regularly used to teach medical students about basic MRI principles in "Principles of Biomedical Imaging" (HST.164).

3. Overview of scanner

The scanners were built as a collaborative effort with a combination of off-the-shelf electronics and in-house developed components. The overall design goal was to enable a fully functional conventional MRI scanner (i.e. conventional gradient encoding without pre-polarization steps) at a cost compatible with educational labs. Fig. 1 shows a photo of a completed scanner with major components labeled. The designs of several components have been modified over time both to improve functionality or to further reduce cost. We will describe the original scanner's components (still in use on the 20 educational scanners) but will also note alternative components and designs.

The system is designed around conventional Fourier imaging of samples in 1 cm NMR tubes. A permanent magnet is used to create the B_0 field of 0.18T in the original magnets and higher in subsequent versions. The Medusa console [16] produces the RF and gradient pulses and acquires the MR signal. The gradient waveforms are amplified by custom compact gradient power amplifiers (GPAs), and then low-pass filtered to remove RF noise before supplying current to the gradient coils. Linear gradient fields (Gx, Gy, Gz) are generated from air-cooled shielded planar gradient coils fabricated as PCB boards. The RF excitation pulses are amplified by an off-the-shelf 1 W power amplifier and passed through a transmit-receive (T/R) switch and into a simple transmit-receive RF coil. The MR signal is amplified by very low-cost preamplifier ICs prior to digitization by the Medusa console's analog-to-digital converter (ADC). MATLAB based GUIs were created for each of the prepared lab exercises. Detailed descriptions of the scanner components and GUIs follow.

4. Magnet – B_0 field

The B_0 magnetic field is produced by a dipole permanent magnet assembly. In clinical MRI scanners, the use of permanent magnet dipole configurations is less common than higher field superconducting designs due to weight and relatively low attainable field strength. However, the size and weight of the permanent magnet dipole scales favorably with Field of View (FOV) allowing the 1 cm FOV tabletop magnet to be lightweight (<20 kg). Additionally, unlike superconducting or resistive electromagnets, permanent magnets require no power and cooling, making them easier to maintain and more robust as educational systems.

High grade Neodymium-Iron-Boron (either N45 or N48 NdFeB) was chosen as the permanent magnet material due to its remnant flux density and magnetic coercivity and relative low cost. One disadvantage of NdFeB is its field dependence with temperature, causing B_0 field drift with normal room temperature fluctuation (-0.12% / K). Practically, this means that the Larmor frequency varies slightly between lab sessions (or even during the session), and students must regularly readjust the frequency in the GUIs to be "on resonance". This temperature drift limited the total practical scan time to ~10 min. However, other solutions to this problem are possible, such as the acquisition of MR navigators to track the drift and

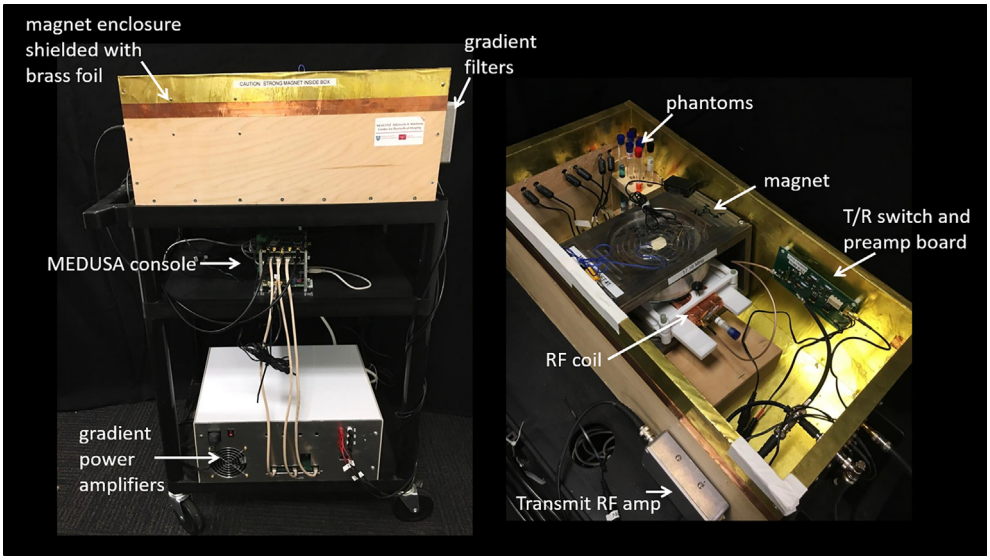

Fig. 1. A complete tabletop MRI scanner is shown on a cart (left). The magnet enclosure is a plywood box lined with brass foil to reduce RF interference (lid not shown). The magnet, gradient coils, RF coil, T/R switch, preamps, and collection of phantoms are located inside the box (right).

generate phase corrections for the raw data. This is an example of a more advanced student project with the scanners.

There are many examples of small permanent magnet assemblies previously constructed for portable NMR and MRI or educational systems [17,18,12,5,19–31,14,32,33,9,34–36], including yokeless Halbach cylinders [19,20,23–25,28,26,29,33,9], yoked dipole magnets [5,22,27,18], and single-sided magnets [12,14,35]. Many of these designs have been previously reviewed [36]. We used a symmetric H-shape dipole yoked design, which tends to produce the most uniform field. The general design is illustrated in Figs. 2 and 3. Two cylindrical NdFeB permanent magnet discs were attached to a high permeability yoke in a dipole configuration. The yoke acts as a frame that contains and guides the magnetic flux, increasing the magnetic field efficiency and concentrating the flux density in the air gap. Pole pieces were attached to the NdFeB faces to shape the field for increased homogeneity. The magnets were designed with a 4 cm gap between the pole pieces, leaving space for the planar gradient coils, RF coil and 1 cm imaging FOV. The yoke shape, NdFeB dimensions, and pole piece shape can all be optimized for a target field and weight. For example, our designs include cylindrical cut-outs in the yoke that increases homogeneity and decreases the overall weight.

Twenty of the magnet assemblies shown in Fig. 2 were produced at the Chinese Academy of Science (CAS) in Beijing. This magnet design yields a 0.18T B_0 field, with < 50 ppm homogeneity (after passive shimming) in the 1 cm FOV. The N45M NdFeB magnet discs are 8 mm thick with a 125 mm diameter. The pole pieces have a tapered shape with 150 mm max diameter. The overall magnet dimensions are 220 mm × 160 mm × 160 mm with a weight of 13 kg. The yoke and pole pieces are made from DT4, electrical pure iron. Additional structural pieces are made from aluminum and POM plastic. The rim shape of the pole piece was optimized for homogeneity.

Additional B0 shimming was done by gluing small (1–4 mm) SmCo pieces to the pole surface. The shimming process was iterative and empirical. The general approach included dividing the ROI into a few layers and mapping the layer to a shimming ring on the pole piece with an empirically chosen dimeter. The iterative process involved shim piece placement followed by field measurements of the ROI. The general process required up to 50 iteration.

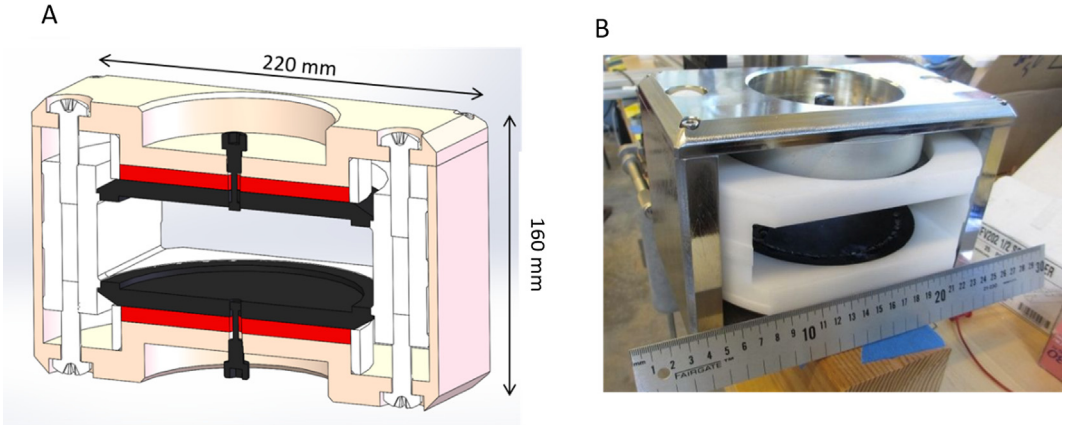

Fig. 2. The CAS magnet used for the 20 educational scanners. The small permanent magnet weighs 13 kg, has a 0.18T B_0 field, 50 ppm homogeneity in the center 1 cm DSV. (A) CAD cross-section view of magnet. The N45M NdFeB material (red) is 8 mm thick with 125 mm diameter. The pole pieces (black) is tapered with a 160 mm max diameter. The yoke (pink) and pole piece are made from DT4, pure electrical iron. The gap between the pole pieces is 4 cm. (B) Photo of the magnet. Small SmCo shim magnets are visible on the pole piece.

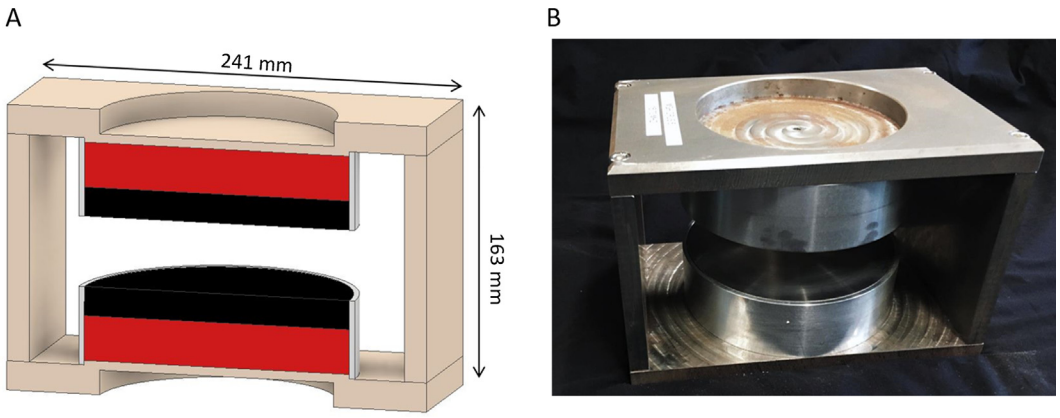

Fig. 3. The alternative MGH magnet design weighs 24 kg and has a 0.37T B_0 field with <40 ppm homogeneity in the 1 cm FOV. (a) CAD cross-section view of magnet. The two NdFeB N48 discs (red) are 25.4 mm thick with a 152 mm diameter. The pole piece (black) and yoke (tan) are made from 1018 low-carbon steel. (A) 4 cm gap is maintained for the gradient coil set and RF coil. (B) Photo of the 0.37T magnet.

Before shimming the field homogeneity was about 300 ppm and could be improved to 20 ppm after shimming.

The alternative magnet design, shown in Fig. 3, was later developed at MGH based on the original CAS design. This magnet uses 152 mm diameter, 25 mm thick (6″ D × 1″) NdFeB N48 discs to produce a higher field of B_0 = 0.37T with < 40 ppm homogeneity in the 1 cm FOV (<20 ppm with linear shim fields). The overall magnet dimensions are 241 mm × 163 mm × 159 mm with a weight of 24 kg. The yoke and pole pieces are made from 1018 low-carbon steel, a readily available material with high tensile strength and high saturation flux density (B_{sat} = 2.42 Tesla). Aluminum rings surround the pole piece, NdFeB discs, and yoke bump-outs ensure proper alignment, improving field homogeneity. The < 40 ppm homogeneity was achievable without passive shimming with accurate alignment of the larger magnet and piece (compared to the CAS magnet).

Assembly of the magnet components was performed with extreme caution on a non-magnetic surface in an area free of loose ferrous objects. These large NdFeB pieces exert high pulling forces (2600 N for the N48 discs) which can cause serious injury. A jig was built to clamp the NdFeB discs while slowly lowering them onto the steel yokes with a screw mechanism. The same jig is then used to slowly attach the steel pole pieces. We previously presented an overview of the MGH magnet simulation and construction process including safety considerations [37].

5. Console

The scaled implementation of the educational scanners required a compact, low-cost console with a convenient PC interface. There have been several low-cost consoles developed for research systems with applications in low-field MRI, portable MRI and relaxometry, as well as educational systems [18,16,5,38–44,6,45–44]. In particular, the maturity of low-cost, large capacity field-programmable gate arrays (FPGAs) or Complex Programable Logic Devices (CPLDs) has been leveraged by several groups to produce small-footprint, low-cost MRI consoles [16,40–44,46,47].

Twenty sets of the modular, scalable Medusa console were fabricated for the educational systems [16]. The Medusa was developed at Stanford University as a modular and scalable console for configurable channel counts in the receiver, transmitter and gradient/shim systems. The console architecture uses a central Controller board to communicate and synchronize up to 16 RF or Gradient modules via a 16-bit parallel data link and communicates with the host PC via USB 2.0. Each Medusa RF module has a receive channel, transmit channel, and gating signals for the amplifiers. The RF module uses an Analog Devices AD9854 DDS and high-speed DACs to directly synthesize RF waveforms from DC to 100 MHz with 14-bit phase control and 12-bit amplitude control. The RF receiver uses an Analog Devices AD6644 14-bit ADC for direct sampling of the RF waveforms. Because the 100–132 MB/s data stream from the AD6644 is impractical for onboard memory storage, an AD6620 Digital Receiver is used for down-mixing and filtering since the MRI signal only occupies a small fraction of the sampling bandwidth (up to 500 KHz). Four digital gradient waveforms can be produced by each Medusa Gradient Module which are then fed via SPI bus to LTC1592 DAC modules to supply analog waveforms to the gradient power amplifiers (GPAs). The Medusa uses a MATLAB extension driver (MEX) and library of functions and tools to support MATLAB user control and pulse sequence design with a simple waveform data format. The library was used to produce the educational MATLAB GUIs described later. In the sequences described here, the console outputs consisted of 80–160 ms "hard" RF pulses (no amplitude or frequency shaping), a transmit gate signal for controlling the RF hardware, and 3 gradient waveforms. In batch mode, the entire pulse sequence is pre-loaded to the Medusa and then executed. However, due to onboard memory limitations, for larger 3D k-space datasets the Medusa was operated in "streaming" mode, where the host computer loads pulse sequence blocks into the Medusa's memory continuously during sequence execution.

While the MEDUSA represents a dedicated, user-friendly design for MRI purposes, there are off-the-shelf FPGA-based development boards or data acquisition systems that can be adapted as MRI consoles. This approach has a cost benefit from wider use and standardization but requires more development resources. However, several groups have used this approach and developed the necessary software and ancillary hardware as open-source projects [6,43–45]. Many are represented on the Open Source Imaging website [48]. For example, the open-source gr-MRI platform extends the functionality of GNU radio software to MRI, allowing console implementation on low-cost software-defined radio (SDR) devices [6]. The OPENCORE NMR is an opensource tool kit for implementing a FPGA-based NMR spectrometer, which is being continually updated (at the time of publication) [44,49]. A modular, open-source platform built on Peripheral eXtensions for Instrumentation express (PXIe) bus was recently introduced and used to implement a console with multichannel RF transmit-receive [45]. Finally, the

Open-source Console for Realtime Acquisitions (OCRA) project aims are to create a low-cost, open-source console capable of real-time control [43].

One of the tabletop scanners has been used as a testbed for the development of the OCRA console at MGH. The console is implemented with a Red Pitaya STEMLab board, a DAC board, and programmable attenuator for less than $500 [50]. The Red Pitaya STEMLab 125-14 board currently sells for $329 USD and uses a Xilinx Zynq 7010 SoC with high-end ADCs (14 bit 125 MS/s) and DACs (14 bit 125 MS/s). The external DAC board was designed with three AD5780 18-bit DACs for the gradient waveforms (Analog Devices, Norwood, MA). The external USB-controlled programmable attenuator (Minicircuits RCDAT-4000-120) was added to the small-signal transmit pulse output to enable RF flip-angle calibrations. The Xilinx Zynq 7010 SoC contains a Xilinx FPGA, dual-core ARM processer and shared RAM, allowing for the implementation of real-time closed loop control of the pulse sequence. The FPGA plays the pulse sequences and the CPU receives real-time updates from the Python-based GUI client and updates the output waveforms. Like the Medusa MATLAB GUIs, GUIs for the OCRA were developed in Python to teach MRI concepts and demonstrate the real-time sequence control capabilities of the console. The OCRA console and GUIs were successfully integrated with one of the tabletop scanners to produce high-quality 1 cm FOV images using both gradient echo and spin-echo pulse sequences. The acquired k-space phase was highly stable from shot-to-shot (provided there was no magnet drift), providing ghost-free images. OCRA is now being used as a tool for testing variants of the tabletop scanner hardware presented here (including some upgraded electronics) by a team of students at the University of Magdeburg in Germany [51]. We refer the reader to the OCRA github page for open-source project resources (https://openmri.github.io/ocra/).

6. RF subsystem

The transmit-receive (T/R) coil is a simple 12 mm diameter, 8 turn solenoid wound with AWG 24 wire on a 3D printed former (Fig. 4). Each coil was tuned to the specific Larmor frequency of the designated scanner and matched to 50 Ω with two sets of high Q capacitors (Knowles/Voltronics, Cazenovia, NY). Fig. 4 shows the coil, capacitors, phantom, and SMA feedthrough mounted in the 3D printed enclosure. RF shielding is implemented by wrapping 0.001″ thick copper foil around the enclosure and grounding to the SMA feedthrough. The shielding reduces RF interference and improves the SNR of the images by a factor of > 5. However, it is important to note that the copper shield shifts the tuning frequency upward and eddy currents may occur if the copper foil is too thick (eddy current-induced gradient delays were observed with 0.005″ foil).

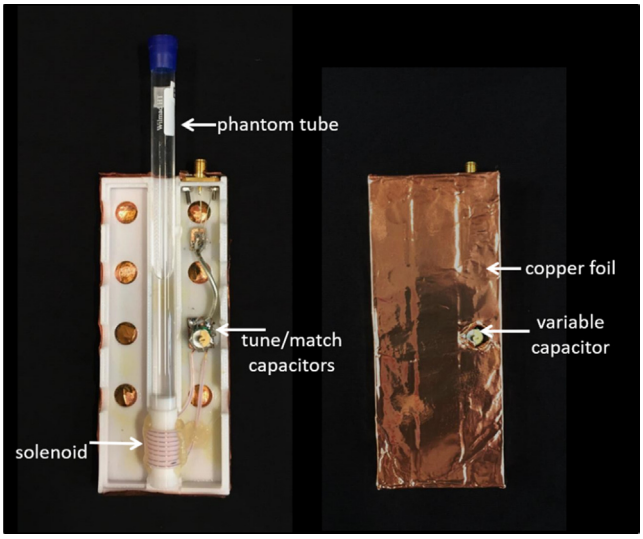

Fig. 4. The RF transmit/receive coil is a 1.2 cm diameter tuned solenoid. The coil is mounted in a 3D printed box wrapped in copper foil for RF shielding. The phantoms are made from water filled 1 cm diameter NMR tubes with inserted 3D printed "plugs" with negative space shapes.

The imaging samples were all made in 1 cm diameter NMR tubes which fit tightly in the 3D printed coil holder. To construct phantoms, the tubes were filled with Gd-doped water, then 3D printed cylinders with negative-space shapes were inserted. Biological samples were also prepared with mouse brains and hearts fixed in formalin, a convenient aqueous solution for imaging since it generates no background signal (HT501128-4L, Sigma-Aldrich, St. Louis, MO, USA).

The active T/R switch is controlled by the console's TX gating signal and laid out on a single PCB with the preamplifier (schematic in Fig. 5a). The T/R switch is a classic PIN diode quarter-wave design. There is a series pin diode between the transmit port and the coil, and a PIN diode shunt to ground protecting the preamplifier. Between the coil and the shunt PIN diode, there is a 50-ohm lumped-element quarter-wave pi-network, which performs an impedance transformation of 180 degree at the Larmor frequency. When the TX gate signal is high, the PIN diodes are forward biased (via a DC current through a bias choke) and in their "short-circuit" state. In this mode, the series PIN diode connects the transmitter to the coil (thru a DC blocking capacitor). The shunt PIN diode (in front of the preamp), grounds the preamp input and this low impedance is transformed by the pi-network to present a high impedance to the RF power amplifier, ensuring that the transmit current goes to the coil. When the PIN diodes are not biased (or reverse biased) they have a high impedance. In this case, the RF coil is isolated from the transmitter and connected by the pi-network to the pre-amplifier. Our design could be improved by providing a reverse DC bias to the PIN diodes during the receive-mode to increase isolation and further decrease noise coupling between from the power amplifier and pre-amplifier.

The preamplifier uses 2 stages of low-cost (< $3 USD) GALI-74+ preamplifier ICs (Mini-Circuits, Brooklyn, NY, USA). The GALI-74+ is a monolithic preamplifier with a 2.7 dB noise figure and 25 dB of gain. After preamplification the signal is filtered by a Mini-Circuits SCLF-10+ low-pass anti-aliasing filter with a 10 MHz cutoff frequency before passing to the Medusa console ADC. Recommended improvements to the T/R switch/preamplifier board include: (1) reverse biasing of the PIN diodes during the receive mode, (2) a crossed diode pair at the preamplifier input to prevent exceeding the max input voltage, (3) using a more robust 2nd stage amplifier with a high max input. There are many alternatives to the Gali-74+ ICs that could be evaluated from Mini-circuits and other vendors. Additionally, custom narrowband preamplifier designs may be beneficial. For example, designs with parallel front-end amplifiers (summing configuration) [52,53] could reduce the overall noise figure.

The transmit RF pulses are amplified by a Mini-Circuits ZHL-3A 29.5 dBm (~1 W) amplifier with 24 dB gain. Alternatively, a 28.5 dBm (~700mW) Motorola MHW592 power amplifier with 35 dB gain has also been used with these systems. In the images, we encountered a DC artifact that was attributable to insufficient isolation between the power amplifier and the coil, allowing the low-level output of the console oscillator to leak through during signal reception. To account for this, a power blanking circuit was implemented for the power amplifier during the receive mode of the system. The blanking circuit, shown in Fig. 5b, includes a voltage regulator (7824) and a simple switch which connects the supply power to the amplifier when the transmit gate signal is high. The MHW592 worked slightly better for fast unblanking since it has

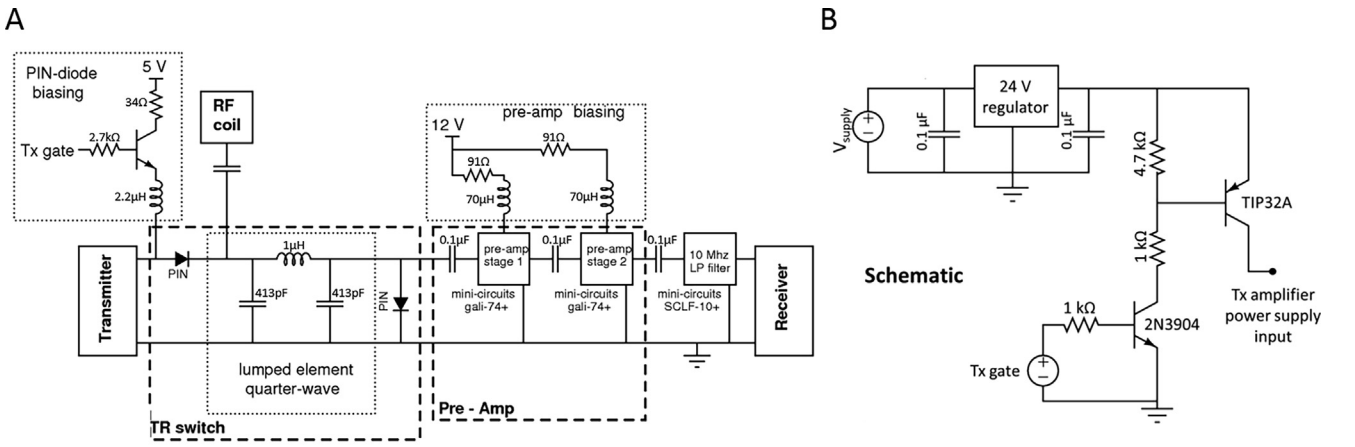

Fig. 5. (A) Combined T/R switch and pre-amplifier schematic. The T/R switch is the classic PIN-diode – λ/4 lumped element design. The pre-amplifier is composed of 2 cascaded Mini-Circuits monolithic low-noise amplifiers. The output of the pre-amplifier is filtered with a Mini-Circuits low-pass filter. (B) Blanking circuit schematic. When the Tx gate signal is high (5 V during the transmit pulses), the circuit's voltage output of 24 V powers the RF transmit amplifier. When the Tx gate signal is low (0 V), the power to the amplifier is "blanked" preventing any RF leak-through during receive-mode.

shorter switching transients after being powered on. However, the power-blanking circuit could also be improved with a push-pull output, where a pull-down transistor would rapidly discharge the power amplifier's filtering capacitors and yield a faster shutoff. We also note that a negative bias on the T/R switch PIN diodes may be an alternative solution to power blanking.

7. Gradient subsystem

The system was designed to use the traditional switchable linear gradient fields, Gx, Gy, Gz. Offset currents to these gradient coils also served as linear shims to improve the B_0 homogeneity. The digital gradient waveforms are passed to the Gradient Power Amplifier (GPA) chassis, which contains the Medusa gradient DAC modules, linear power supplies, and GPA boards. The amplified gradient waveforms are low-pass filtered by differential Butterworth filter modules at the entrance to the system's shielded box. Finally, the amplified, filtered waveforms drive the planar gradient coils to encode the image and shim the B_0 field.

The gradient coils were implemented as shielded planar coils, with two primary coils and two shielding coils for the X, Y, Z, and Z2 terms (the Z2 coil was included for B_0 shimming but has not been utilized). Active shielding of the gradient coils was added to prevent eddy current formation in the magnet pole pieces. The coil design was based on the stream function method [54]. The design was optimized with three objective functions. The first objective function aimed for a target field with linear B_z components in the 1 cm spherical FOV and zero field on the magnet pole piece surfaces. Another design objective was minimization of the coil power dissipation in order to operate without water cooling. The third objective maintained sufficient space for the trace width by minimizing the p-norm ($p > 2$) of a surface current density [55]. The optimization problem including those three objectives is converted to a single-objective problem using the weighted sum method. The single-objective problem was then solved by the limited-memory BFGS method [56] which is implemented in a MATLAB function of minFunc [57].

The optimized current traces were fabricated on printed circuit boards (PCBs). To minimize the resistance, 2 oz (71 μm thick) copper was used with a minimum trace width of 2 mm. In total, the coils were implemented on four 8-layer PCBs (1 primary and 1 shielding board per pole-piece). Each of the 4 coils (Gx, Gy, Gz and Z2) in each board had 2 layers; a "wind-in" and a "wind-out" layer connected with buried vias (thus 8 layers total). The 8 copper traces for the primary coil board are shown in Fig. 6. The shielding boards were placed immediately adjacent to the pole pieces (2 cm from isocenter) and the primary boards were 1 cm from isocenter, leaving approximately 2 cm for RF coil enclosure. A plastic 3D printed frame was designed to stack and space the PCBs properly in the magnet. Fig. 6b shows this structure and the gradient coil stack. The gradient efficiency of the coils is; 13.7 mT/m/A, 10.4 mT/m/A, and 12.3 mT/m/A for Gx, Gy and Gz respectively. Similarly, the impedance of each coil is [10.3 μH, 0.385 Ω], [10.4 μH, 0.365 Ω], and [6.4 μH, 0.188 Ω].

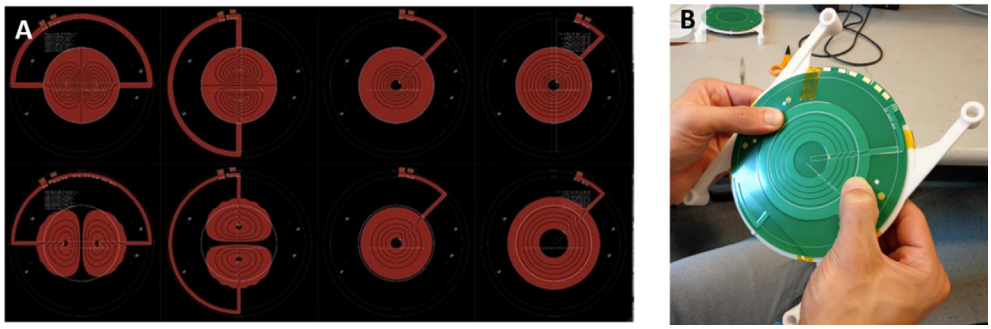

Fig. 6. The air-cooled shielded planar gradient coils were fabricated as PCBs. (A) Copper traces for X, Y, Z, and Z2 coils primary coils and shielding coils. The traces were optimized for linear fields in the 1 cm ROI and zero field at the magnet poles (to prevent eddy currents). (B) Photo of gradient coil stack with plastic holder to be inserted in the 4 cm magnet gap.

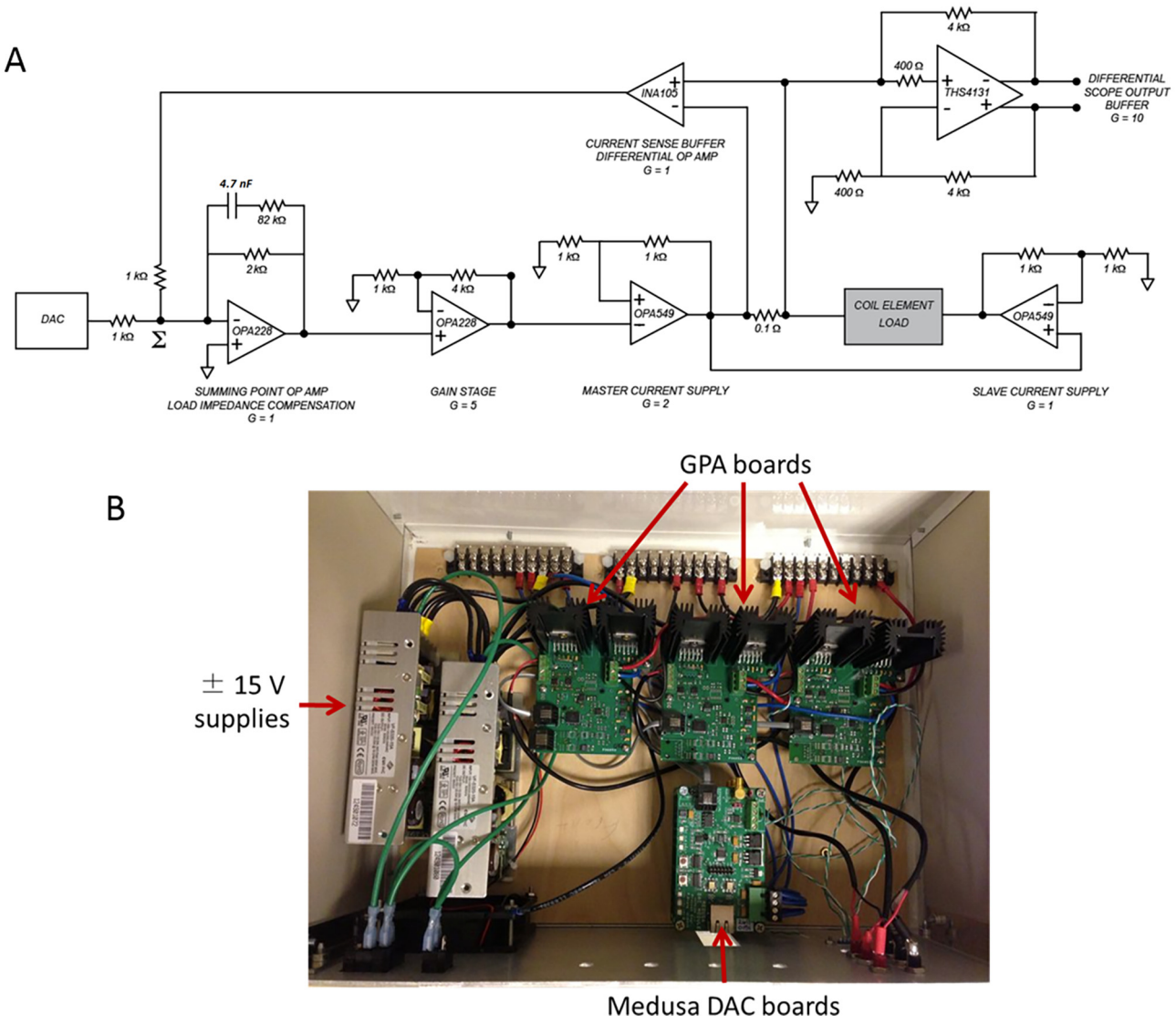

Fig. 7. (A) Gradient power amplifier (GPA) schematic. A master-slave op-amp configuration is used to drive the gradient coils. The voltage across a 0.1 current sense resistor is buffered and used in a feedback loop to maintain a constant current output which is proportional to the voltage input from the DAC. (B) The gradient power amplifier (GPA) chassis contains the Gx, Gy, and Gz amplifier boards, the 15 V power supplies, and the digital to analog converter boards.

The design goal for the gradient power amplifier was to create an inexpensive, easy to fabricate amplifier capable of driving the gradient coils with a least 5 amps of current over a 10 kHz bandwidth. Fig. 7 shows the GPA schematic. It uses low-cost, fault-protected OPA549 op-amps (Texas Instruments, Dallas, TX) in a push-pull (class A-B) configuration. The devices were powered from ±15 V rails supplied by an inexpensive switching power supply. The voltage across a 0.1 Ω current sense resistor is buffered with a TI-INA105 precision difference amplifier, and used in the feedback loop to maintain a true constant current output proportional to the control input voltage. The TI-OPA228 summing point op amp adjusts its output to penalize any difference between the input signal voltage and the feedback loop current sense voltage in order to hold the output current constant in the presence of disturbances (such as coupling from other slewing gradient coils). The capacitors and resistors in the summing point op amp's own negative feedback loop compensate for the phase delay imparted by the load impedance and the transfer functions of the op amps used in the circuit, in order to ensure stable output. A differential scope output is included to monitor the buffered current sense resistor voltage. This allows students to view the gradient currents either with an oscilloscope or with a data acquisition card. Bench tests show that the current output tracks the input control signal with high fidelity and short achievable rise times. Driving the ~10 μH gradient coils (0.4Ω resistance), the GPAs switch from 0 to 3 amps in <30 μs.

In addition to the design above, other GPA designs have been prototyped and tested, including a circuit adapted from a motor controller topology with an integrated DAC that can operate with a single-supply rail [15,58]. The board file and schematic for this V2 design is included in the supplementary material.

8. Graphical user interfaces (GUIs) and sequences

The MEDUSA console was controlled with MATLAB, permitting easy control of the tabletop imaging experiments and processing of the output data. Graphical User Interfaces (GUIs) are used as "wrappers" around the sequences in order to permit users to easily change experimental parameters, acquire data, and perform basic

data processing in real time. Data can be saved from the GUIs to allow students to perform signal processing exercises offline (e.g., FFT, sampling, filtering, etc.). Four basic GUIs are used for experiments with the tabletop scanners. The FID GUI allows users to find the initial signal and determine the center frequency, shim currents, and RF power levels to use subsequently. The Spin-echo/projection GUI uses these settings to acquire a simple spin-echo with an adjustable TE. Each of the gradient fields can be turned on during the spin-echo acquisition to acquire projections of the sample. The 2D imaging GUI uses a cartesian spin-echo sequence in single-echo mode (one echo per TR) and displays the raw kspace data line by line in real-time. Echo train mode (RARE imaging) is also an option with the 2D imaging GUI. In this case, the acquisitions use 6/8 partial Fourier with a 72 echo train to zero pad out to a 96 × 96 in-plane image matrix. Effective TE = 72 ms and echo spacing is 2.9 ms. Finally, the 3D imaging GUI uses a RARE sequence to acquire images with the user specified FOV, number of partitions, and TR. The same acquisition parameters as the 2D RARE sequence are used with the addition of the third dimension phase encode loop. More information about the GUIs and lab exercises is provided in the supplementary material (Supplementary data 2).

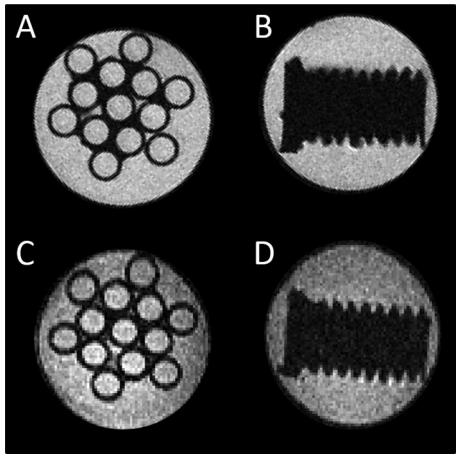

Fig. 9. (A and B) Phantom images acquired with a Bruker 4.7T animal scanner. RARE sequence, RARE factor = 16, res = 0.1 mm × 0.1 mm × 0.75 mm. BW = 50 kHz, NA = 2. (C-D) Images acquired with the tabletop scanner. 3D RARE sequence, FOV = 1.3 cm, partition thickness = 1.25 mm, image matrix = 96 × 96 × 16, 6/8 partial Fourier, BW = 62 kHz, NA = 8. (A and C) Capillary tubes with 1.8 mm OD and 150 μm wall thickness. Bruker SNR = 23, Tabletop SNR = 16. (D) Nylon bolt with a thread spacing of 0.7 mm. Bruker SNR = 23. Tabletop SNR = 13.

9. Results

Figs. 8 and 9 demonstrate the imaging performance with the tabletop MRI scanner. Fig. 8a, shows resulting 2D phantom images using 10 averages of the 2D RARE sequence described above. The phantoms consist of 3D printed plastic shapes inserted into the 1 cm NMR tubes filled with water. Fig. 8b–c show 3D images acquired with the 3D RARE sequence described above. The phantom imaged in Fig. 8b consisted of three separate 2 mm plastic letters stacked in the NMR tube. Fig. 8c shows a 3D image of an ex-vivo mouse brain fixed in formalin.

Fig. 9 shows a comparison of the tabletop MRI imaging performance (Fig. 9C and D) with a Bruker 4.7T animal scanner (Fig. 9A and B). Figure A and C shows images of a phantom containing several capillary tubes with a 1.8 mm outer diameter and a 150 μm wall thickness. Figure B and D shows images of a nylon bolt with a 0.7 mm pitch (thread spacing). These phantom tubes were filled with isopropyl alcohol. The Bruker scan used a RARE sequence with slice selection and 2 averages. The acquired resolution was 0.1 mm × 0.1 mm × 0.75 mm. The tabletop scan used the 3D RARE sequence with 6/8 partial fourier and 8 averages. The acquired resolution was 0.135 mm × 0.135 mm × 1.25 mm. The average SNR in the Bruker images is 23 and the average SNR in the tabletop images is 15. The tabletop images show some distortion, a ~ 5% stretch in the Y direction. This likely due to gradient calibration errors.

The lower SNR in the tabletop images is expected due to the 13X lower B_0 field strength. However, these images demonstrate an imaging performance that is more than adequate for teaching and many research purposes. Notably, we can easily resolve the 150 μm wall thickness in the capillary tubes in Fig. 9C.

10. Conclusion

The low-cost educational tabletop scanner and MATLAB GUIs described here have been successfully used by > 800 students for several years to teach fundamental concepts in engineering, signal processing, and MR physics. The described system and GUIs offer a basic introduction these subjects, but more advanced design projects can be undertaken by interested students and researchers. In addition to a structured teaching tool, these systems serve as an accessible prototyping platform for MR engineering research projects. Here we present a snapshot of the open-source component designs and implementation that will continue to evolve over time as students and researchers take on projects using the scanner as a platform. To enrich this effort, the authors would welcome contributions of designs for upgraded/updated hardware modules and GUI software from members of the MR research community who adopt the platform in their own teaching.

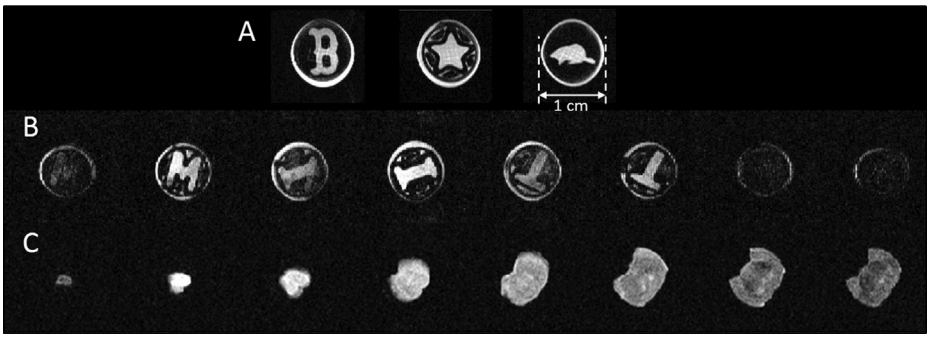

Fig. 8. (A) 2D RARE acquisitions on tabletop scanner of a few representative 2D-phantoms (FOV = 1.75 cm, matrix = 96x96x1, NA = 10). (B–C) 3D RARE images. (B) 3D-printed "M-I-T" phantom image (FOV = 2 cm in-plane, 2.5 cm through-plane, matrix = 96 × 96 × 8, NA = 1). (C) Mouse brain (FOV = 1.75 cm in-plane, 1.5 cm through-plane, matrix = 96 × 96 × 8, NA = 32). All acquisitions use 6/8 partial Fourier with 72 echo train to zero pad out to 96 × 96 in-plane image matrix. Effective TE = 72 ms and echo spacing is 2.9 ms.

Declaration of Competing Interest

The authors declare that they have no known competing financial interests or personal relationships that could have appeared to influence the work reported in this paper.

Acknowledgments

The authors would like to thank Collin Stultz, Anantha Chandrakasan, Alan Jasanoff, Steven Wasserman, Susie Huang, David Sosnovik, Melissa Haskell, Jeff Stout, Erica Mason, Patrick McDaniel, Filiz Yetisir, Simon Sigalovsky, Bo Zhu, Nick Arango, Monika Sliwiak, Eric Gale, Iris Yuwen Zhou and Marcus Prier. We acknowledge the Department of Electrical Engineering and Computer Science at MIT (USA) for funding the purchase of parts and equipment for MIT-MGH tabletop scanners. Manuscript preparation was supported by the MGH Office of Women's Careers Scholary Writing Award (USA). This work was supported by the German Research Foundation (DFG) (Grant Number ZA 422/5-1) (Germany). Research reported in this paper was supported by the National Institute of Biomedical Imaging and Bioengineering (NIBIB) of the National Institutes of Health under award number R01EB018976 and K99EB021349 (USA). The content is solely the responsibility of the authors and does not necessarily represent the official views of the National Institutes of Health.

Appendix A. Supplementary material

Supplementary data to this article can be found online at https://doi.org/10.1016/j.jmr.2019.106625.

References

[1] J. Braun et al., A compact 0.5 T MR elastography device and its application for studying viscoelasticity changes in biological tissues during progressive formalin fixation, Magn. Reson. Med. 79 (1) (2018) 470–478.
[2] T. Haishi, T. Uematsu, Y. Matsuda, K. Kose, Development of a 1.0 T MR microscope using a Nd-Fe-B permanent magnet, Magn. Reson. Imaging 19 (6) (2001) 875–880.
[3] T. Shirai, T. Haishi, S. Utsuzawa, Y. Matsuda, K. Kose, Development of a compact mouse MRI using a yokeless permanent magnet, Magn. Reson. Med. Sci. 4 (3) (2005) 137–143.
[4] N. Iita, S. Handa, S. Tomiha, K. Kose, Development of a compact MRI system for measuring the trabecular bone microstructure of the finger, Magn. Reson. Med. 57 (2) (2007) 272–277.
[5] S.M. Wright et al., A desktop magnetic resonance imaging system, Magn. Reson. Mater. Phys. Biol. Med. 13 (3) (2001) 177–185.
[6] C.J. Hasselwander, Z. Cao, W.A. Grissom, gr-MRI: A software package for magnetic resonance imaging using software defined radios, J. Magn. Reson. 270 (2016) 47–55.
[7] Bernhard Blümich, Low-field and benchtop NMR, J. Magn. Reson. 306 (2019) 27–35, https://doi.org/10.1016/j.jmr.2019.07.030.
[8] E. Danieli, J. Perlo, B. Blümich, F. Casanova, Small magnets for portable NMR spectrometers, Angew. Chem. Int. Ed. 49 (24) (2010) 4133–4135.
[9] P. Yu, Y. Xu, Z. Wu, Y. Chang, Q. Chen, X. Yang, A low-cost home-built NMR using Halbach magnet, J. Magn. Reson. 294 (Sep. 2018) 162–168.
[10] J. Anders, K. Lips, MR to go, J. Magn. Reson. San Diego Calif 1997 306 (2019) 118–123.
[11] Y.-Q. Song, S. Utsuzawa, Y. Tang, Low fields but high impact: Ex-situ NMR and MRI, J. Magn. Reson. San Diego Calif. 1997 306 (2019) 109–111.
[12] R.S.G. Eidmann, The NMR MOUSE, a mobile universal surface explorer, J. Magn. Reson. Ser. A 122 (1996) 104–109.
[13] M.N. Martin, B.J. Balcom, M.J. McCarthy, M.P. Augustine, Noninvasive, nondestructive measurement of tomato concentrate spoilage in large-volume aseptic packages, J. Food Sci. 84 (10) (2019) 2898–2906.
[14] A. Bashyam, M. Li, M.J. Cima, Design and experimental validation of Unilateral Linear Halbach magnet arrays for single-sided magnetic resonance, J. Magn. Reson. 292 (2018) 36–43.
[15] Tabletop MRI development page. [Online]. Available: https://tabletop.martinos.org.
[16] P.P. Stang, S.M. Conolly, J.M. Santos, J.M. Pauly, G.C. Scott, Medusa: a scalable MR console using USB, IEEE Trans. Med. Imaging 31 (2) (2012) 370–379.
[17] Portable Educational MRI System - Niumag. [Online]. Available: http://en.niumag.com/portable-educational-mri-system.html. (Accessed: 24-Jun-2019).
[18] Pure Devices GmbH, Pure Devices Magnet, 2013. [Online]. Available: http://pure-devices.com/html/magnet.html. (Accessed: 23-Jul-2014).
[19] G. Moresi, R. Magin, Miniature permanent magnet for table-top NMR, Concepts Magn. Reson. Part B Magn. Reson. Eng. 19B (1) (2003) 35–43.
[20] H. Raich, P. Blümler, Design and construction of a dipolar Halbach array with a homogeneous field from identical bar magnets: NMR Mandhalas, Concept Magn. Reson. Part B 23B (1) (2004) 16–25.
[21] N.R. Routley, K.J. Carlton, The HALO system—a light weight portable imaging system, Magn. Reson. Imaging 22 (8) (2004) 1145–1151.
[22] A.V. Sahakian, C. Hayes, B. Yalvac, An inexpensive laboratory module to teach principles of NMR/MRI, ASEE Annu Conf. Expo.Conf. Proc. (2005) 8007–8016.
[23] B.P. Hills, K.M. Wright, D.G. Gillies, A low-field, low-cost Halbach magnet array for open-access NMR, J. Magn. Reson. 175 (2) (2005) 336–339.
[24] E. Danieli, J. Mauler, J. Perlo, B. Blümich, F. Casanova, Mobile sensor for high resolution NMR spectroscopy and imaging, J. Magn. Reson. 198 (1) (2009) 80–87.
[25] H. Soltner, P. Blümler, Dipolar Halbach magnet stacks made from identically shaped permanent magnets for magnetic resonance, Concepts Magn. Reson. Part A 36A (4) (2010) 211–222.
[26] C. Hugon, F. D'Amico, G. Aubert, D. Sakellariou, Design of arbitrarily homogeneous permanent magnet systems for NMR and MRI: Theory and experimental developments of a simple portable magnet, J. Magn. Reson. 205 (1) (2010) 75–85.
[27] S.M. Wright, M.P. McDougall, J.C. Bosshard, A desktop imaging system for teaching MR engineering, in: presented at the Annual International Conference of the IEEE Engineering in Medicine and Biology Society (EMBC), 2010, pp. 6653–6656.
[28] C. Windt, H. Soltner, D. van Dusschoten, P. Blumler, A portable Halbach magnet that can be opened and closed without force: The NMR-CUFF, J. Magn. Reson. 208 (1) (2011) 27–33.
[29] E. Danieli, J. Perlo, B. Blümich, F. Casanova, Highly stable and finely tuned magnetic fields generated by permanent magnet assemblies, Phys. Rev. Lett. 110 (18) (2013) 180801.
[30] M.C.D. Tayler, D. Sakellariou, Low-cost, pseudo-Halbach dipole magnets for NMR, J. Magn. Reson. 277 (2017) 143–148.
[31] K. Chonlathep, T. Sakamoto, K. Sugahara, Y. Kondo, A simple and low-cost permanent magnet system for NMR, J. Magn. Reson. 275 (2017) 114–119.
[32] B. Blümich, K. Singh, Desktop NMR and its applications from materials science to organic chemistry, Angew. Chem. Int. Ed. 57 (24) (2018) 6996–7010.
[33] C.Z. Cooley et al., Design of sparse halbach magnet arrays for portable MRI using a genetic algorithm, IEEE Trans. Magn. 54 (1) (2018) 1–12.
[34] Z.H. Ren, W.C. Mu, S.Y. Huang, Design and optimization of a ring-pair permanent magnet array for head imaging in a low-field portable MRI system, IEEE Trans. Magn. 55 (1) (2019) 1–8.
[35] P.C. McDaniel, C.Z. Cooley, J.P. Stockmann, L.L. Wald, The MR Cap: A single-sided MRI system designed for potential point-of-care limited field-of-view brain imaging, Magn. Reson. Med. (2019).
[36] M. Johns, E.O. Fridjonsson, S. Vogt, A. Haber, Mobile NMR and MRI: Developments and Applications, Royal Society of Chemistry, 2015.
[37] J.P. Stockmann, Maker B0 - educational session, in: Proceedings of the Annual Meeting ISMRM 2018, Paris, 2018. [Online]. Available: https://cds.ismrm.org/protected/18MPresentations/abstracts/E1193.html.
[38] M. Twieg, M.J. Riffe, N. Gudino, M.A. Griswold, An Open Source Mobile NMR Relaxometry Platform, in: Proc. 21st Annu. Meet. ISMRM Salt Lake City Utah USA 2013, p. 0139, 2013.
[39] T. Kimura et al., Development of a mobile magnetic resonance imaging system for outdoor tree measurements, Rev. Sci. Instrum. 82 (5) (2011) 053704.
[40] W. Tang et al., A home-built digital optical MRI console using high-speed serial links, Magn. Reson. Med. 74 (2) (2015) 578–588.
[41] X. Liang, S. Binghe, M. Yueping, Z. Ruyan, A digital magnetic resonance imaging spectrometer using digital signal processor and field programmable gate array, Rev. Sci. Instrum. 84 (5) (2013) 054702.
[42] W. Mao et al., A modularized pulse programmer for NMR spectroscopy, Meas. Sci. Technol. 22 (2) (2010) 025901.
[43] S. Anand, J.P. Stockmann, L.L. Wald, T. Witzel, A low-cost (<$500 USD) FPGA-based console capable of real-time control, in: Proc. Jt. Annu. Meet. ISMRM-ESMRM 2018 Paris, p. 0948, 2018.
[44] K. Takeda, OPENCORE NMR: open-source core modules for implementing an integrated FPGA-based NMR spectrometer, J. Magn. Reson. San Diego Calif. 1997 192 (2) (2008) 218–229.
[45] A. Ang, M. Bourne, R. Dykstra, An open source PXIe ecosystem based on FPGA modules, in: 2017 International Conference on Field Programmable Technology (ICFPT), 2017, pp. 219–222.
[46] S. Jie, X. Qin, L. Ying, L. Gengying, Home-built magnetic resonance imaging system (0.3 T) with a complete digital spectrometer, Rev. Sci. Instrum. 76 (10) (2005) 105101.
[47] W.K. Peng, L. Chen, J. Han, Development of miniaturized, portable magnetic resonance relaxometry system for point-of-care medical diagnosis, Rev. Sci. Instrum. 83 (9) (2012) 095115.
[48] Open Source Imaging Initiative (OSI2). [Online]. Available: https://www.opensourceimaging.org/. (Accessed: 12-Jun-2019).
[49] Opencore NMR 2. [Online]. Available: http://kuchem.kyoto-u.ac.jp/bun/indiv/takezo/opencorenmr2/. (Accessed: 18-Jun-2019).
[50] Red Pitaya STEMlab board. [Online]. Available: https://www.redpitaya.com/f130/STEMlab-board. (Accessed: 17-Jul-2018).
[51] O. Speck (personal communication).
[52] A. Malhotra, T. Buzug, Op-amp based low noise amplifier for magnetic particle spectroscopy, Curr. Dir. Biomed. Eng. 3 (2017).

[53] W. Zhang, B. Zheng, P. Goodwill, S. Conolly, A custom low-noise preamplifier for Magnetic Particle Imaging, in: 2015 5th International Workshop on Magnetic Particle Imaging (IWMPI), 2015, p. 1.
[54] G.N. Peeren, Stream function approach for determining optimal surface currents, J. Comput. Phys. 191 (1) (2003) 305–321.
[55] F. Jia, S. Littin, K.J. Layton, S. Kroboth, H. Yu, M. Zaitsev, Design of a shielded coil element of a matrix gradient coil, J. Magn. Reson. 281 (Aug. 2017) 217–228.
[56] J. Nocedal, S.J. Wright, Numerical optimization, Springer, New York, 2006.
[57] minFunc - unconstrained differentiable multivariate optimization in Matlab. [Online]. Available: https://www.cs.ubc.ca/~schmidtm/Software/minFunc.html. (Accessed: 28-Jun-2019).
[58] N. Arango, J.P. Stockmann, T. Witzel, L.L. Wald, J. White, Open-Source, Low-Cost, Flexible, Current Feedback-Controlled Driver Circuit for Local B0 Shim Coils and Other Applications, in: Proc. Annu. Meet. ISMRM 2016 Singap, p. 1157, 2016.
[59] P.C. Lauterbur, Image formation by induced local interactions: examples employing nuclear magnetic resonance, Nature 242 (5394) (1973) 190–191.